Available online at www.sciencedirect.com
SCIENCE DIRECT®
Journal of Power Sources 128 (2004) 45–53
JOURNAL OF POWER SOURCES
www.elsevier.com/locate/jpowsour

Engineered cathodes for high performance SOFCs

R.E. Williford*, P. Singh

Pacific Northwest National Laboratory, PO Box 999, Mail Stop K2-44, Richland, WA 99352, USA

Received 21 August 2003; accepted 15 September 2003

Abstract

Computational design analysis of a high performance cathode is a cost-effective means of exploring new microstructure and material options for solid oxide fuel cells. A two-layered porous cathode design has been developed that includes a thinner layer with smaller grain diameters at the cathode/electrolyte interface followed by a relatively thicker outer layer with larger grains at the electrode/oxidant interface. Results are presented for the determination of spatially dependent current generation distributions, assessment of the importance of concentration polarization, and sensitivity to measurable microstructural variables. Estimates of the electrode performance in air at 700 °C indicate that performance approaching 3.1 A/cm^2 at 0.078 V is *theoretically* possible. The limitations of the model are described, along with efforts needed to verify and refine the predictions. The feasibility of fabricating the electrode configuration is also discussed.
© 2003 Published by Elsevier B.V.

Keywords: Solid oxide fuel cells; Cathodes; Microstructure

1. Introduction

A solid oxide fuel cell (SOFC) is composed of a dense electrolyte sandwiched between porous electrodes. The key electrochemical reactions occur mostly on the *surfaces* at the electrolyte/electrode interfaces, thus enabling the harvesting of electrons in an electrical circuit to produce useful power. The dense electrolyte conducts oxygen ions from the cathode to the anode, but prevents mixing of the fuel and oxidant in the *gas* phase, where electrons cannot be harvested. The porous electrodes permit passage of the gases to the electrolyte/electrode interfaces where the reactions occur. A relatively thick porous anode is often used to provide structural support for the assembly. The cathode is often relatively thin to minimize its contribution to the overpotential by polarization losses. It is generally recognized that a significant portion of these polarization losses originate in the cathode. Consequently, much attention has recently been focused on improving cathode performance through two means: improved materials and improved microstructural designs. Improved materials include mixed ionic electronic conductors (MIECs), which essentially increase the surface area available for conversion of gaseous oxygen molecules to oxygen ions. Such a material has been developed in our laboratory [1], and was employed in this work. The present paper focuses on methods to improve the microstructural design of the cathode.

An objective of this work is to design a solid oxide fuel cell (SOFC) cathode exhibiting a low area specific resistance (ASR = 0.1 Ω cm^2) and capable of high current output. Such an objective can be attained best by a coupled experimental-modeling approach: the modeling helps to guide the experiments and the experiments provide data for fitting the parameters of the model. Since modeling is often cheaper than a long series of Edisonian experiments, costs are often minimized with this approach. This paper describes modeling efforts and includes selected experimental data, which are reported in more detail elsewhere [1].

An initial step was to review the existing models in the literature, and select an approach that was both pragmatic and thorough, in addition to exhibiting direct linkages with the experimental data. We found four categories of models, which are described below in terms of complexity and input data requirements. The following paragraphs are not an exhaustive review, and contain only representative examples of each model type.

In the first category are detailed models by Svensson et al. [2]. This model treats the classic three phase boundary (TPB) problem explicitly by addressing the individual mechanisms involved (surface adsorption, dissociation, electronic exchange, surface diffusion). Non-linear second order differential equations are derived and solved numerically, with the proper boundary conditions (six are required). Although the model certainly contains enough technical depth,

* Corresponding author. Tel.: +1-509-375-2956; fax: +1-509-375-2186.
E-mail address: rick.williford@pnl.gov (R.E. Williford).

0378-7753/$ – see front matter © 2003 Published by Elsevier B.V.
doi:10.1016/j.powsour.2003.09.055

it also requires the estimation of about a dozen parameters (such as surface diffusion coefficients) that generally have uncertainties of two to four orders of magnitude. Estimation of these parameters would require an extensive series of well-controlled experiments, at appreciable cost. This model was not suitable for the present program. Similar conclusions have been reached elsewhere [3].

In the second category are models based on a homogenized, effective medium concept for the porous cathode material [4,5]. The TPB mechanisms described above are lumped into a single parameter called the surface exchange coefficient (K_s, cm/s), which is experimentally measurable on a routine basis, e.g. [6]. A significant database exists in the literature for a range of mixed ionic electronic conductors (MIEC) that are important in the present effort. In this respect, the models in [4,5] are suitable because of the direct connection to experimental tasks. However, two factors present problems. The first was the mathematical complexity resulting from treatment of four polarization terms (Butler–Volmer, chemical resistance caused by the exchange process, concentration polarization, and gas capacitance at the cathode/gas interface). Second, communication with the author [4,5] indicated that several typographical errors existed in the literature, thus requiring re-derivation of the model to ensure correctness. The investment required for this type of model also rendered it unsuitable for the present work.

In the third category are models by Deng et al. (DZA) [7] (without concentration polarization), and [8] (with concentration polarization). These models use the same surface exchange concept as in [4,5], but treat only the chemical resistance term [7] and the concentration polarization term [7,8]. Numerical input requirements are comparatively modest, and the models are mathematically tractable. Although solutions are available in closed-form, these solutions are for a homogeneous material, so that spatially variant material properties are not treated. Consequently, numerical solutions of the differential equations will ultimately be required for multilayered cathode concepts. The models are also well suited for the high conductivity materials used in this investigation, and were selected for the calculations herein.

In the fourth category are the more classical models, e.g. [9], which generally treat all polarization terms in a semi-empirical manner. They require input of a modest amount of experimental data, most of which is available, and are mathematically tractable. However, linearizations in the model have apparently caused the loss of important effects, particularly for gas diffusion through the porous material. The manifestation of this problem was the rather high values derived for the tortuosity, indicating that several unknowns and uncertainties had numerically accumulated in this parameter. This type of model was thus not suitable for the present effort.

We selected the models by Deng et al. (DZA) [7,8] for this work because of their direct relationship to experimental measurables, treatment of the two most important polarization terms, mathematical tractability, and the availability of closed-form solutions for initial estimates. The following paragraphs describe preliminary results using these models.

2. Engineered cathode development

2.1. Estimation of current distribution

In the early stages of this investigation, the lanthanum strontium copper ferrite (LSCuF) cathode material being tested exhibited very low ASR and high current. It was therefore thought that concentration polarization was negligible up to about 0.1 V. The DZA [7] model was extended to permit estimation of possible oxygen potential gradients, and used to estimate the current distribution throughout the cathode material. Model parameters are defined in Appendix A, and the model details are given in Appendix B, along with a benchmark case for LSCoF.

Preliminary results for the very efficient mixed ionic electronic conductors (MIECs) under consideration indicated that most of the ionic current was generated near the cathode/electrolyte interface (at $x/L = 1$), as shown in Fig. 1 for a single layer of LSCuF. The approximately 5–8 μm region of high current generation is larger than the usual three phase boundary width discussed in the literature, probably because of errors in the estimated material parameters at this early stage in the analysis. The results are very sensitive to the pore surface area/volume ratio (S) defined in Appendix A. Although the results are consistent with LSCuF performance at low overpotentials, a detectable amount of concentration polarization was indicated, which motivated the next stage of the analysis.

2.2. Material properties and microstructural sensitivities of the model

The second DZA model [8] also treated concentration polarization along with the polarization due to chemical resistance (R_{ch}), and is briefly summarized in Appendix C.

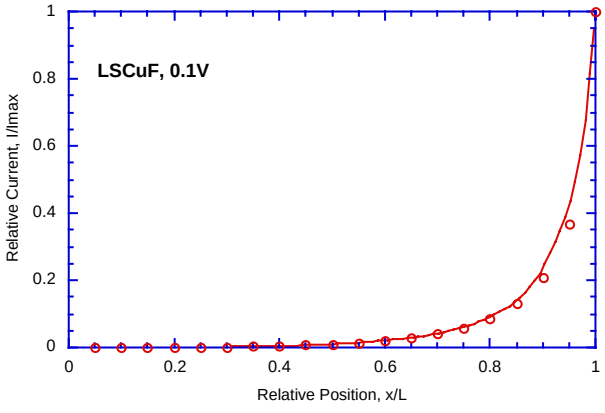

Fig. 1. Current distribution in a homogeneous LSCuF cathode.

A second computer simulation code was constructed using this model. The code has three main functions: (a) fitting to experimental *V–I* data to extract the value of the surface exchange coefficient directly from the performance data, (b) variation of model parameters to reveal the sensitivities to microstructural variables, and (c) computation of the current and voltage as a function of position in the cathode material.

Although the closed-form solution provided by this model is very useful, its limitation is that it treats only homogeneous materials. That is, the microstructural parameters may not depend on spatial position. It will be seen that a piecewise numerical solution of the model is required for the final design of the cathode.

Analysis using the extraction mode was applied to one of the best performing materials developed in this laboratory: LSCuF. The operating parameters were $T = 700\,^{\circ}\mathrm{C}$ and $P_{O_2} = 2.12 \times 10^4$ Pa (air) [1]. The ionic and electronic conductivities were taken as 0.01 and 100 S/cm, respectively. The thickness was 25 μm, porosity 50%, grain size 1 μm, pore size 1 μm, with solid and gas tortuosities of 1.89 and 2.5 (see Appendix C). Several dozen runs revealed that the best ionic diffusivity value was 5×10^{-8} cm^2/s, which is slightly higher than that for LSC and LSCoF (1×10^{-8} to 2×10^{-8}) [6], but still quite reasonable in light of the chemically active role copper plays in many technologies (e.g., getters, superconductivity, etc.). This is probably due to the electronic structure of copper, analysis of which is outside the scope of this work.

The solutions for K_s for the various current and voltage data pairs are shown in Fig. 2. The curve labeled curs_p (with concentration polarization) reproduces the data at an ASR of about 0.06 Ω cm^2 in the ohmic regime, and shows the apparent concentration polarization becoming important above about 0.1 V as the non-polarized (curs_np) curve departs noticeably from curs_p. When compared to the solid material (cur_s), both curves show the significant enhancement provided by the porous material. L_p (the characteristic length of the three phase region) at 0.1 V was 1.7 μm and L_g (the characteristic length for concentration polarization) was 113 μm, indicating minimal concentration polarization at this voltage (see Appendix A for definitions of parameters). The P_{O_2} at the cathode/electrolyte interface had fallen to 1.52 Pa at 0.1 V. The value of K_s at 0.1 V was 2.17×10^{-6} cm/s, which is quite reasonable compared to that for LSC and LSCoF at 700 °C (3×10^{-6} to 4×10^{-6} cm/s).

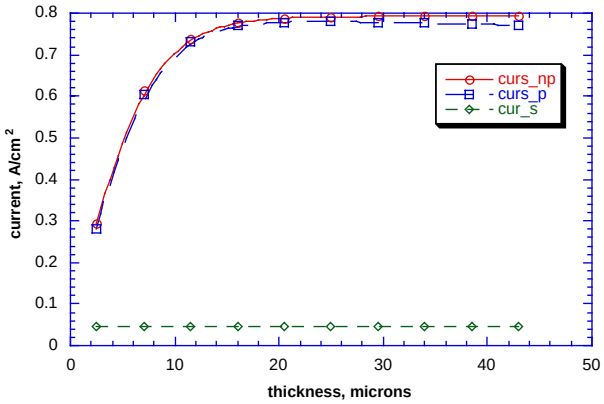

Fig. 3. Effect of varying cathode thickness with all other parameters held constant: overvoltage = 0.1 V.

The above results were then used in the model's sensitivity mode to study the impact of varying microstructural parameters as follows. Fig. 3 shows the effect of varying the cathode thickness. It appears that the present 25 μm thickness is just sufficient to establish a stable enhancement of current due to the ion collection activity of the outer regions of the MIEC cathode material. At thicknesses greater than 25 μm, concentration polarization effects become noticeable.

Variations in porosity cause variations in the pore surface area/volume ratio (S) and the tortuosities, and are shown in Fig. 4. Although the enhancement remains significant, it is interesting that a lower porosity results in a higher current. This may be due to part of the particular relationship (see Appendix C) between the ionic diffusivity and the surface exchange coefficient. The characteristic distance

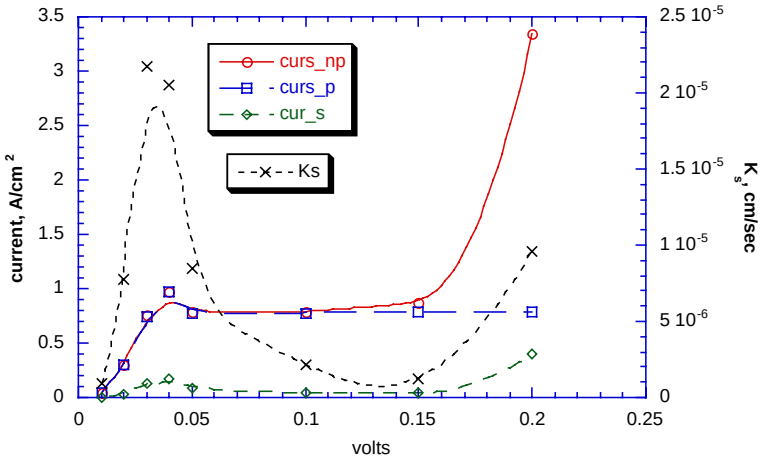

Fig. 2. Analysis of LSCuF data in the extraction mode. The squares are the experimental data points. The long-dashed curve is the model fit to the data. Other symbols are explained in the text.

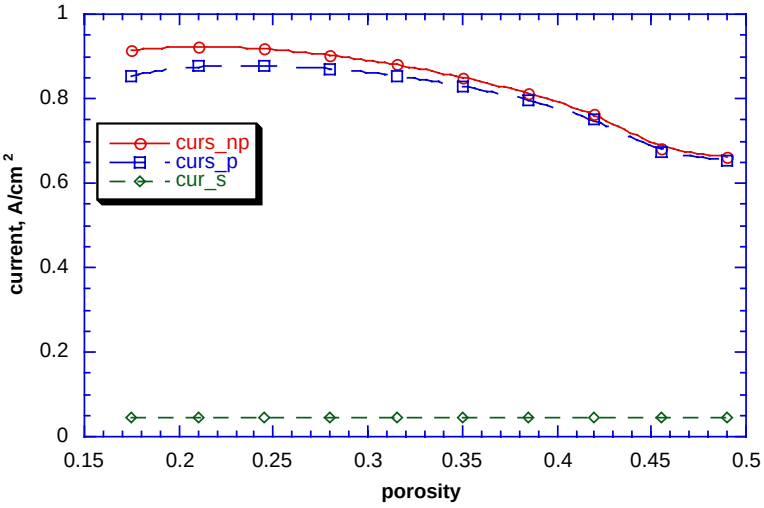

Fig. 4. Effect of varying porosity at 0.1 V overvoltage.

for the transition between reactivity and diffusion dominance was $L_d = 230\,\mu m$. Another data set and associated benchmarking exercise may indeed give different results. For the present combination of parameters, at 0.1 V overvoltage, it appears that lower porosity may give a slightly higher current. However, this enhancement is smaller than that provided by other microstructural parameters, as shown below.

The pore surface area decreases when grain diameter increases, but the tortuosities are not greatly affected in the present formulations. The decreasing pore surface area reduces the total ionic current, as shown in Fig. 5.

Fig. 6 shows that variations in pore diameter have negligible effect in this regime because the micron-sized pores are greater than the mean free path of the molecules, thus minimizing the Knudsen effect.

The conclusion was that smaller grain diameters would provide the greatest increase in currents, e.g., reducing the grain size from 1.0 to 0.25 μm could double the current.

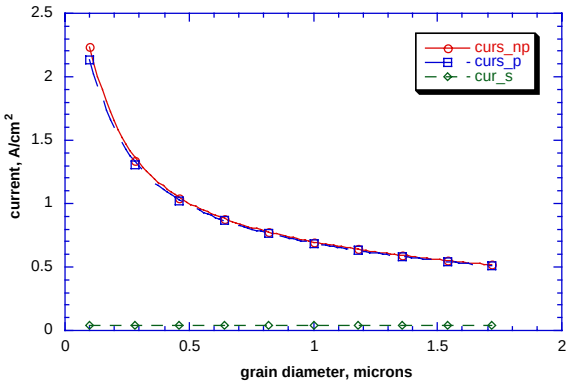

Fig. 5. Effect of grain size on currents at 0.1 V overvoltage.

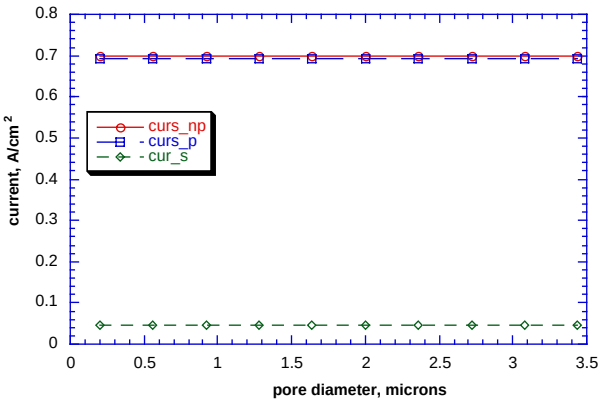

Fig. 6. Effect of varying pore diameters at 0.1 V overvoltage.

3. Design optimization for a two-layer cathode

The above results indicated that the most effective way to increase the current output of the cathode was to decrease the grain size, while maintaining the porosity at a high level. This means that the cathode internal pore surface area to cathode volume ratio will rise appreciably. It also means that the cathode will be a very fragile structure, and difficulties may be expected in attaching current collectors to its outer surface. One solution to this problem is to employ a two-layer cathode system: a more structurally robust outer layer with larger grains and an inner layer (next to the electrolyte) with smaller grains. The outer layer should have enough porosity to easily transport a steady supply of air/O_2 to the more chemically active inner layer. The following design is based on the above cited material properties extracted from experimental data (0.78 A/cm^2 at 0.1 V). The only change is that the base porosity was reduced to 45% to take advantage of the small enhancement

in Fig. 4, and to ensure numerical stability in the calculations.

The design of each layer is described below. It is important to note how the model was applied in these cases. Each layer was treated as an individual cathode, i.e., the model was applied twice, once for the outer layer and once for the inner layer. This was necessary because of the single-material limitations of the model. Thus, the results should be considered as approximate until they can be confirmed by more detailed analysis with a model that treats the spatial variation of material properties explicitly.

3.1. Outer layer

The following microstructural parameters were defined: thickness = 25 μm, porosity 45%, pore diameter = 1 μm, grain diameter = 1 μm, surface/volume ratio S = 50,000 cm^{-1}, gas tortuosity = 2.22, solid tortuosity = 1.83 (effective path for ionic and electronic conduction). Results are shown in Fig. 7.

The 5 μm active region adjacent to the electrolyte (at x = 0) is evident. The P_{O_2} at the 5 μm distance was estimated to be 1.62×10^4 Pa, the overvoltage (η) 4.69×10^{-3} V, and the ionic current 0.0106 A/cm^2. These values define the boundary conditions for the inner layer, at the inner/outer layer interface. While the overvoltage and current at the 5 μm position are good numbers, it is important to note that the P_{O_2} value was very approximate. This is because of limitations in the closed-form solution of the model, which did not supply a solution for the oxygen chemical potential for this particular geometry. It was thus necessary to estimate the P_{O_2} using a Nernstian approximation, which will be improved upon in later work.

Two designs for the inner layer are discussed next, the objective of which is to increase the current output above that seen for the single layer in Fig. 7.

3.2. Inner layer

3.2.1. Small grain diameter (0.25 μm)

Because of the smaller grains, the surface/volume ratio is increased to $S = 1.22 \times 10^6$ cm^{-1}. The pore diameter and gas tortuosity were unchanged, but the solid tortuosity is reduced to 1.67. Fig. 8 shows that it is theoretically possible to increase the output of the two-layered cathode to about 3.1 A/cm^2 at 0.078 V. The P_{O_2} at the cathode/electrolyte interface is about 5.17×10^2 Pa using the above mentioned Nernst estimation method, indicating that concentration polarization was not dominant. In the figure, recall that curs_np is the current with no accounting for concentration polarization, curs_p accounts for concentration polarization, cur_s is the current for a solid material, and η is the overvoltage.

However, there is some question that this design may not be manufacturable: the smaller grains require lower sintering temperatures, and overlaying a larger-grained 20 μm thick outer layer would require higher sintering temperatures that would over-sinter the inner layer. For this reason, a design was also generated for an inner layer with a larger grain size.

3.2.2. Larger grain diameter (0.5 μm)

The surface/area ratio for this design was 62,777 cm^{-1}, the solid tortuosity was 1.65, and the P_{O_2} at the cathode/electrolyte interface was less than 1×10^{-5} Pa by the Nernstian approximation. Because of the low P_{O_2}, the calculation actually failed at 0.4 μm from the interface. Fig. 9 shows that the overvoltage was appreciably higher (0.12 V), although the actual current output may achieve values near those of the 0.25 μm grain case at the interface proper. However, the interface would probably be oxygen-starved, thus eliminating any benefit from oxygen impingement directly on a chemically stable thin layer (i.e., 1 μm ceria) between the electrolyte and LSCuF cathode material.

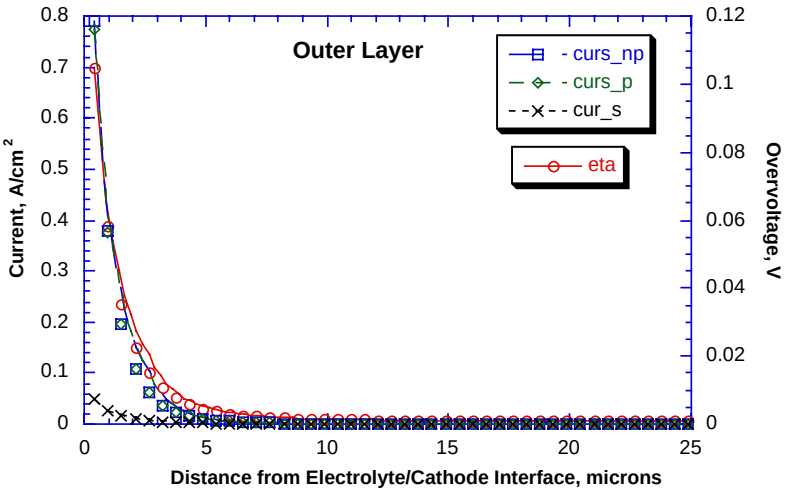

Fig. 7. Ionic current and overvoltage for the cathode outer layer.

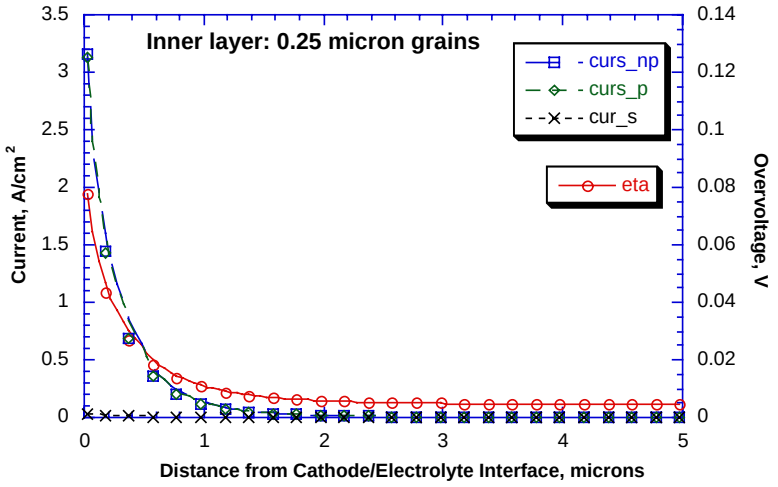

Fig. 8. Ionic current and overvoltage (eta) for the small grain inner layer.

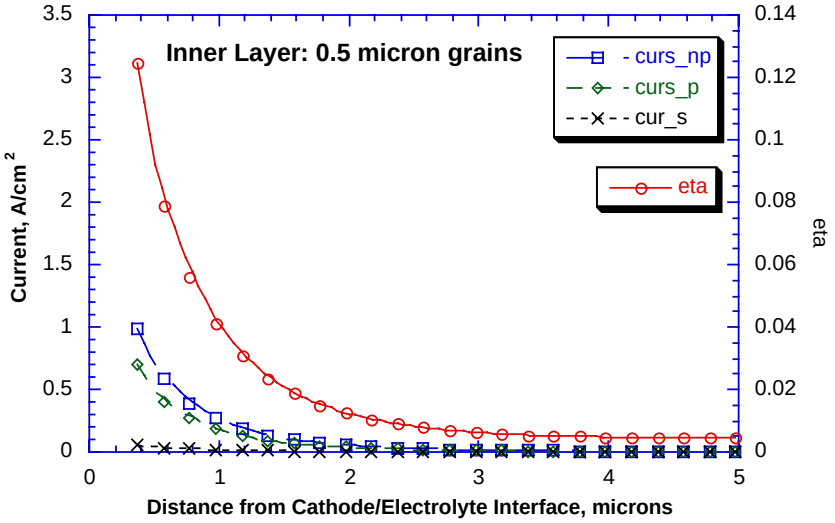

Fig. 9. Ionic current and overvoltage (eta) for the cathode inner layer with larger grain diameter.

It appears that the best design is the 0.25 μm grain, 5 μm thick inner layer. However, the manufacturability of this design must be proven experimentally.

4. Conclusions

The models employed to this point are suitable for a homogeneous material where the properties and microstructures do not vary spatially. However, the microstructural design of the two-layered cathode described above has extended these closed-form models appreciably beyond their intended range of application, and should be considered as approximate.

The candidate material LSCuF investigated in this analysis has exhibited a high affinity for oxygen, and may be suitable for a cathode material if structural and chemical stability can be maintained during long-term high power density operations at elevated operating temperatures. Experimental efforts are underway to investigate the stability of this material, and will be reported in a separate paper.

Acknowledgements

The work described in this report was performed for DARPA under contract MDA972-01-C-0067. Work performed by Pacific Northwest National Laboratory which is operated by Battelle Memorial Institute for the US Department of Energy under contract DE-AC06-76RLO1830. The authors wish to thank Drs. Nguyen Q. Minh and Rajiv Doshi (GE Power Systems) for technical discussions, Dr. V. Browning (DARPA) for support and encouragement, and Mr. G. Coffey and Mr. E. Thompson for their experimental contributions.

Appendix A. Model parameters

The microstructural parameters are:

- the porosity, ϕ;
- the grain diameter, d_g;
- the pore diameter, d_p;
- the internal pore surface area per unit volume, S;
- the thickness of the cathode, L;
- the solid tortuosity for electronic or ionic conduction, t_s;
- the tortuosity for diffusion of the gas in the pores, t_g.

Operational parameters that can be varied:

- the overvoltage, V;
- the total gas pressure at the cathode surface, P_{tot};
- the P_{O_2} at the external surface of the cathode;
- the operating temperature, T.

Material properties input to the model:

- the ionic diffusivity for oxygen, D_{ion};
- the electronic and ionic conductivities, σ_e and σ_I;
- the surface exchange coefficient, K_s;
- the ambipolar diffusion coefficient, $D_{IE} = D_{ion}/(1 + \sigma_I/\sigma_e)$;
- the ionic concentration in the solid material, C_i;
- the characteristic distance for the transition between reactivity and diffusion domination, $L_d = D_{IE}/K_s$;
- the characteristic length of the three phase boundary region, or region of high reactivity near the cathode/electrolyte interface, L_p;
- the characteristic length for concentration polarization effects, L_g;
- the chemical resistance due to ionic conduction and surface exchange, R_{ch}.

Calculated output from the model:

- the ionic current for a solid material, I_I^s;
- the ionic current for a porous material with no concentration polarization, I_{np};
- the ionic current for a porous material including concentration polarization effects, I_p;
- the ASR of the cathode material, given by the current divided by the overvoltage.

Appendix B

The DZA model [7] for small concentration polarization is summarized as follows.

The ionic current for a solid material is defined as

$$I_I^s = \frac{K_s C_i \Delta\mu_g}{RT}, \tag{B.1}$$

where

$$\Delta\mu_g = \frac{RT}{4} \ln\left(\frac{P_{O_2\,\text{external}}}{P_{O_2\,\text{interface}}}\right). \tag{B.2}$$

The corresponding current for a porous material is given by

$$I_i(x) = I_I^s M G(x), \tag{B.3}$$

where the material factor is

$$M = \frac{L_d S(1-\phi)}{\tau_s}, \tag{B.4}$$

and G is a geometric factor given by

$$G(x) = \frac{a\exp[(L-x)/L_p] + \exp[x/L_p]}{a\exp[L/L_p] + 1}, \tag{B.5}$$

where x is the distance from the cathode/electrolyte interface, and

$$a = \frac{1+u}{1-u}, \tag{B.6}$$

$$u = \left[\frac{\tau_s(1-\phi)}{SL_d}\right]^{1/2}, \tag{B.7}$$

and

$$L_p = \left[\frac{L_d(1-\phi)}{S\tau_s}\right]^{1/2}. \tag{B.8}$$

Eq. (B.3) describes the ionic current in the porous solid in the Gerisher limit, where the oxygen potential is constant. The source of this ionic current is the oxygen molecular flux through the pores: the molecular current is converted to ionic current through the surface exchange mechanism. The molecular flux through the pores can be expressed as:

$$I_g = -\frac{\phi}{\tau_g D_g}\frac{dC_g}{dx}, \tag{B.9}$$

where D_g is the diffusivity of the O_2 in the pores (corrected for Knudsen effects) and C_g is the concentration of the O_2 in the pores, which depends on position x in the porous material. When all the molecular O_2 is converted to ionic current, we have

$$I_g = \tfrac{1}{2} I_{I\,(max)}. \tag{B.10}$$

But this does not admit spatial dependence of P_{O_2}.

To obtain that spatial dependence, we depart from the original developments by DZA [7], as follows. Note that at any position x, the time rate of change of the molecular current is proportional to the spatial gradient in the ionic current:

$$\frac{dI_g}{dt} = -\frac{1}{2}\frac{dI_I}{dx}. \tag{B.11}$$

From the continuity equation, we also have

$$\frac{dI_g}{dt} = -\frac{dI_g}{dx}. \tag{B.12}$$

Substituting Eqs. (B.3), (B.9) and (B.12) into Eq. (B.11) results in a second order differential equation in the oxygen partial pressure as a function of spatial position x. This is a two-point boundary value problem, and is integrated numerically by a relaxation method. The numerical solution is

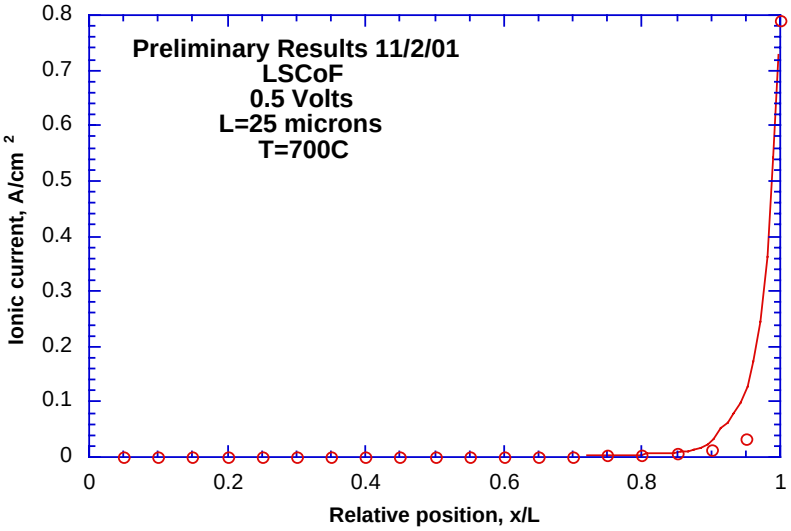

Fig. 10. Benchmark case for LSCoF at 0.5 V, $L = 25\,\mu m$, $T = 700\,^{\circ}C$.

then substituted into the Nernst equation (since concentration polarization is expected to be negligible) to obtain an estimate of the local overpotential between two points $x(i)$ and $x(i-1)$:

$$\eta = \frac{RT}{4F} \ln\left[\frac{P_{O_2}(x(i))}{P_{O_2}(x(i-1))}\right]. \tag{B.13}$$

The chemical resistance R_{ch} (or ASR for no concentration polarization) is calculated from

$$R_{ch} = \frac{RT}{2F^2 K_s C_{ion}} \left(\frac{\tau_s}{L_d S(1-\phi)}\right)^{1/2}, \tag{B.14}$$

and the current increment between $x(i)$ and $x(i-1)$ is calculated from Ohm's law, including the geometric factor G for the ionic flux, by

$$\Delta I(x(i)) = \frac{\Delta\eta(x(i))}{R_{ch} \times G(x(i))}. \tag{B.15}$$

The current increments are then added to find the local current as a function of position. The method was benchmarked using a case for LSCoF discussed in detail in Ref. [5]. Results (shown in Fig. 10) indicate that the majority of the current is generated within about 2.5 μm of the cathode/electrolyte interface (at $x/L = 1$), in reasonably good agreement with the previous calculation of $L_d = 3\,\mu m$, shown in Fig. 8a of [5]. Results for LSCuF are shown in the main text.

Appendix C

C.1. Microstructural design including concentration polarization

The second DZA model [8] solved two coupled differential equations for the chemical potential μ of the ambipolar (ion + electron) species and for the chemical potential μ of the oxygen molecules, as a function of position x in the porous cathode material. The ionic current is given by

$$I_p = -\frac{1-\phi}{\tau_s} \frac{D_{IE} C_i}{RT} \frac{d\mu}{dx}, \tag{C.1}$$

where

$$\mu - \mu_0 = \left[g_{11} \exp\left(-\frac{x}{L_m}\right) + g_{12} \exp\left(\frac{x}{L_m}\right)\right] \Psi_{11} + [g_{21}x + g_{22}]\Psi_{12} - \Delta\mu_g, \tag{C.2}$$

where μ_0 is the ambipolar chemical potential at the cathode/electrolyte interface ($x = 0$), and the g_{ii} are constants determined from the boundary conditions The g_{ii} equations are several pages long and are not repeated here. Several typographical errors in the original publication have been corrected for the present work. The Ψ_{ii} are components of the eigenvector matrix, and L_m is given by

$$\frac{1}{L_m^2} = \frac{1}{L_p^2} + \frac{1}{L_g^2}, \tag{C.3}$$

where

$$L_g = 2L_p \left[\frac{\tau_s}{\tau_g} \frac{\phi}{1-\phi} \frac{D_g}{D_{IE}} \frac{C_g}{C_i}\right]^{1/2} \tag{C.4}$$

is the characteristic length for concentration polarization to occur, i.e., if this length is smaller than the cathode thickness concentration polarization is important. $\Delta\mu_g$ is the molecular chemical potential difference between the two surfaces of the cathode.

It is important to note that mathematical relationships between the microstructural parameters ϕ, S, τ_s, and τ_g have

been derived for cubic systems in [10], and were also employed in this analysis:

$$S = \frac{3b(1-\phi)}{r_g}, \tag{C.5}$$

where

$$r_g = \tfrac{1}{2}d_g, \tag{C.6}$$

$$b = \frac{1-3q}{1-\frac{9q^2}{2}\left(1-\frac{q}{3}\right)}, \tag{C.7}$$

$$1-\phi = \frac{3\pi/4[2/9 - q^2(1-q/3)]}{(1-q)^3}, \tag{C.8}$$

$$\tau_s = \frac{2}{\pi}(1-\phi)(1-q)\ln\left(\frac{2}{q}-1\right), \tag{C.9}$$

$$\tau_g \simeq \frac{1}{\phi}, \tag{C.10}$$

and q is the fractional consolidation of the grains, a sintering parameter.

This model thus provides a closed-form, simultaneous solution for the two polarization terms of interest in this work, chemical and concentration polarization. Although very useful (see main text), its limitation is that it treats only a homogeneous material. That is, the microstructural parameters are not dependent on spatial position.

References

[1] G.W. Coffey, J. Hardy, O. Marina, L.R. Pederson, P.C. Rieke, E. Thompson, Solid State Ionics, submitted for publication.
[2] A.M. Svensson, S. Sunde, K. Nisancioglu, J. Electrochem. Soc. 145 (1998) 1390.
[3] G.W. Coffey, L.R. Pederson, P.C. Rieke, J. Electrochem. Soc. 150 (2003) A1139.
[4] S.B. Adler, J.A. Lane, B.C.H. Steele, J. Electrochem. Soc. 143 (1996) 3554.
[5] S.B. Adler, Solid State Ionics 111 (1998) 125.
[6] H.J.M. Bouwmeester, A.J. Burgraaf, in: P.J. Gellings, H.J.M. Bouwmeester (Eds.), Table 14.2 CRC Handbook of Solid State Electrochemistry, CRC Press, Boca Raton, 1996, pp. 482–553.
[7] H.M. Deng, M.-Y. Zhou, B. Abeles, Solid State Ionics 74 (1994) 75–84.
[8] H.M. Deng, M.-Y. Zhou, B. Abeles, Solid State Ionics 80 (1995) 213–222.
[9] J.W. Kim, A.V. Virkar, K.Z. Fung, K. Mehta, S.C. Singhal, J. Electrochem. Soc. 146 (1999) 69.
[10] M.-Y. Zhou, P. Sheng, Phys. Rev. B 39 (16) (1989) 12027.